Nanoparticle encapsulation of HDACi with HA targeting in endometrial cancer models

Kadie Edwards
Swansea University Medical School https://orcid.org/0000-0002-1359-0359
Seydou Yao
Swansea University Medical School
Simone Pisano
Swansea University Medical School
Veronica Feltraccao
Swansea University Medical School
Katja Brusehafer
Swansea University Medical School
Sumanta Samanta
Tampere University and BioMediTech Institute
Oommen P Oommen
Tampere University and BioMediTech Institute
Salvatore Andrea Gazze
Swansea University Medical School
Roberta Paravati
Swansea University Medical School
Holly Maddison
Swansea University Medical School
Chao Li
Xi'an Jaotong University
Deyarina Gonzalez
Swansea University Medical School
R. Steven Conlan
Swansea University Medical School
Lewis W Francis (✉ L.francis@swansea.ac.uk)
Swansea University Medical School https://orcid.org/0000-0002-7803-7714

Research

Keywords: pluronic-HA, HDACi, SAHA, nanomedicine, endometrial cancer

Posted Date: July 24th, 2020

DOI: https://doi.org/10.21203/rs.3.rs-45475/v1

Abstract

Bespoke nanoparticle systems can enhance drug delivery, preventing systemic exposure by modifying release kinetics and increasing tumour penetration. Flexible nano vector systems have led to selective tumour targeting through surface modifications and the addition of target moieties over expressed in the cancer microenvironment. As such nanomedicines are enabling drug re-purposing and renewed applications in solid tumour cancers. Here we present the nanoscale encapsulation of Vorinostat within a F127 Pluronic polymer particle modified to incorporate a Hyaluronic Acid moiety, targeting increased CD44 expression in endometrial cancer cells. Encapsulation within a stable micellar structure stabilized SAHA activity, demonstrating increased cytotoxic efficacy in 2-D and 3-D cultures. In addition, nano delivery enhanced spheroid penetration, suppression in cell growth, P21 associated cell cycle arrest and overcome EMT associated phenotype formation observed in the free drug treated type II Hec50 cells. Together, this study clearly demonstrates that HDAC nanoparticle encapsulation and HA targeting may offer a solution to overcoming the toxicity and side effects issues observed in clinical trials. Given the demonstrated involvement of epigenetic processes in oncology, this study is an important demonstration of this class of anti-cancerous agents for the treatment of endometrial cancers.

1. Background

A great volume of work has been committed to the application of nanotechnology to improve cancer diagnosis, imaging and pharmaceuticals. Bespoke nanoparticles as drug delivery vectors have the capacity to enhance drug solubility, prevent systemic exposure and improve delivery to afflicted tissues through modified release profiling [1]. Targeting CD44 with Hyaluronic Acid (HA), this study presents a flexible, biocompatible nano formulation that increases histone deacetylase inhibitor efficacy in 3D endometrial cancer spheroid models.

Endometrial cancer is the sixth most common cancer in women and the 15th most commonly occurring cancer worldwide with over 380,000 new cases reported in 2018 [2–4]. The disease is most prevalent in post-menopausal women, however there has been a dramatic 21% increase in the incidence in the UK between 2005–2015. Alarmingly this rate is exacerbated in younger women aged 25 to 45 years [3, 5], and has been linked to genetic factors, obesity, poor diet, elevated risk in patients suffering from polycystic ovary syndrome [6, 7].

Endometrial cancer can broadly be divided to type I or II, with disease progression further defined in 6 stages, according to the Rotterdam criteria [8]. Type I endometrioid adenocarcinoma, representing 80% of all cases [9], is a low-grade, hormone receptor positive disease with a good prognostic outcome if diagnosed early [7]. Many stage I cancers can be cured with surgery alone, although more advanced stages require adjuvant radiotherapy to avoid reoccurrence [10]. In contrast, type II endometrial carcinomas are estrogen-independent, often with high-grade serous or clear cell histology and poor outcomes, and account for 40% of all endometrial cancer associated mortality [5, 11]. Advanced stage endometrial cancers become metastatic, to the point where surgery is not the most appropriate treatment.

Chemotherapy then becomes the preferred treatment, with cisplatin, carboplatin, doxorubicin and taxane treatment alone or in combination used as the most common treatment regimes, alongside hormone therapies such as megestrol for Type I responsive cancers [12].

Evidence [13, 14] has shown that differences exist in the molecular pathogenesis of type I and II endometrial cancer and links have been established to alterations in epigenetic processes such as DNA (de)methylation [15], histone (de)methylation or (de)acetylation [16, 17]. Nieminen et al. [13], identified 24 tumour suppressor genes that were progressively hypermethylated during the development of type I endometrial cancer [15, 18, 19]. Similarly, treatment of endometrial cancer models using small chemical compounds that modify epigenetic processes can partially, or even fully, restore the normal expression levels of genes including the re-expression of inactivated tumour suppressor genes and deactivation of activated oncogenes [20, 21].

This epigenetic plasticity and the deregulation of epigenetic processes in endometrial cancer, led to the evaluation of suberoylanilide hydroxamic acid (SAHA), currently approved for the treatment of lymphoma and myelodysplastic syndromes, in endometrial cancer clinical trials [22]. SAHA inhibits class I and II HDACs by binding to the Zn2 + chelation centre in the enzyme and affects processes that lead to cell cycle arrest and apoptosis [23–25]. However, in Phase II studies SAHA has demonstrated little to no efficacy either alone or in combination with standard anti-cancer treatments [26]. Several factors may cause the lack of HDAC response, low stability in the blood stream (two-hour elimination half-life) and an inability to accumulate adequate concentrations at the tumour site, a combination of increased drug efflux pump activity and low tumour penetration [27]. Furthermore, the pharmacology of SAHA is particularly complex as they can act as enzyme inducers and may modify their own kinetics [26].

Strategies to overcome such limitations include the development of nanovectors to increase drug stability and passive accumulation of drug-containing nanoparticles at tumour sites, acting as an enhanced tumour targeting agent [1, 28–32]. The improvement of safety and tolerability by nanoparticle-formulated drugs is exemplified by liposomal doxorubicin [33], where increased concentrations of the therapeutic agent accumulate specifically in the tumour [34], by virtue of the purported enhanced permeability and retention effect [35, 36]. Previously, SAHA encapsulation and prodrug approaches have been shown to improve the drug efficacy in melanoma and breast cancers [37, 38]. Such prodrug approaches however limit the application for multiple cargos without complex chemistry in each formulation.

Polymers provide an excellent platform for nanovector systems, with many polymer nanoparticle developments reported for the treatment of solid tumours [39, 40]. Pluronic® F-127 is a water soluble, triblock copolymer consisting of poly(ethylene oxide)-poly(propylene oxide)-poly(ethylene oxide) repeats (PEO101-PPO56-PEO101) that possess a low toxicity *in vivo*, and is FDA approved [41]. F127 nanoparticles have been developed for the controlled release of therapeutic drugs, peptides and proteins [42–44] and with carboxylic groups to mediate the addition of tumour targeting moieties such a folate [45, 46]. An alternative targeting moiety, HA is a naturally occurring glycosaminoglycan that consists of N-acetyl-d-glucosamine and d-glucuronic acid repeat units and is a ligand for the CD44 receptor. CD44 is

found at low levels on the surface of epithelial cells and is highly expressed in endometrial tumours, playing a key role in tumour development and progression [47, 48].

Here we demonstrate the suitability of HA targeted SAHA nanoparticles in 2-D and 3-D cultured endometrial cancer cell line models. Pluronic® F-127-HA polymer encapsulation enhanced SAHA cytotoxicity *in vitro* through delayed release kinetics in both 2-D and 3-D models of type I (Ishikawa) and type II (Hec50) endometrial cancer. Surface conjugation of hyaluronic acid further increased the cytotoxicity of SAHA in both cell types, that demonstrate distinct patterns of CD44 expression. Encapsulation did not affect the mechanism of action, as cellular phenotype, cell cycle checkpoint protein expression and histone H3 acetylation were similarly modified using the free and encapsulated drug in both 2D and 3D cell models. Using SAHA as an exemplar for this exciting class of epigenetic drugs, these data suggest that F127 encapsulation may offer a solution to overcoming the toxicity and off-target effects observed in clinical trials.

2. Results And Discussion

The focus of the work is to demonstrate, for the first time, the utility of HA mediated endometrial cancer targeting using F-127 Pluronic as a nanovector system. HA conjugation to Pluronic® F-127 is assessed for its effect on particle size, stability, drug encapsulation and release. SAHA-F-127-HA particles are then assessed for their efficacy in 2D and 3D culture models of both type I and type II endometrial cancer, characterising drug mechanism of action using both protein expression and histone specific acetylation patterns at key cell cycle checkpoint gene loci. A diagrammatic pipeline of this multidisciplinary study is shown in Fig. 1.

2.1 SAHA dose selection

Ishikawa and Hec50 are accepted and widely used cell lines representative of type I and type II endometrial cancers respectively [49]. In order to select a relevant treatment concentration of SAHA for F-127 encapsulation, we first assessed the *in vitro* cytotoxicity of free SAHA using RTGlo assessment of cellular viability in both endometrial cell lines. Ishikawa and Hec50 2D monolayers were treated with an increasing dose of SAHA concentration (1 μM to 20 μM) over a 96-h time course (Fig. 2).

Type I and type II cell models displayed different response profiles to SAHA treatment, with a significant effect seen with Ishikawa cells at notably lower concentrations compared to Hec50, consistent with previous reports [22, 50, 51]. No significant reduction in Ishikawa cell viability was observed following treatment with 1 μM SAHA after 48 h ($p > 0.05$). At increasing concentrations, significant 57% cell death (1.5 μM; $p > 0.05$) up to 99% cell death (20 μM; $p < 0.001$) were observed. Hec50 cells demonstrated 13%, 46% and 95% cell death following 1 μM, 2.5 μM ($p < 0.05$) and 20 μM ($p > 0.001$) treatments respectively. Using the 72 h data series, the half-maximal inhibitory concentration (IC50) was determined to be 1.2 μM and 2.7 μM for Ishikawa and Hec50 respectively. Having established the response profiles to SAHA

exposure, 2.5 μM was selected for all further treatments, as this was the lowest concentration where a significant reduction in viability was observed for both cell types.

Type II endometrial carcinomas often present as high-grade serous or clear cell histology, with poor outcome, accounting for 40% of all endometrial cancer associated mortality [5, 11]. CD44 protein expression was characterized in both Ishikawa and Hec50 cell lines, using confocal laser scanning microscopy (CSLM; see **Figure S1**). CD44 expression was shown to be consistent throughout the Hec50 population with a relative fluorescence units (RFU) of 0.375 or a cellular RFU of 7.5×10^{-3} (**Figure S1**). In comparison only 43% of Ishikawa cells assessed were shown to be CD44+, with a whole population RFU of 0.204. Notably, this heterogenous expression is highlighted by the increased RFU per cell (10.7×10^{-3}). These two cell lines therefore represent an excellent model of high and low CD44 expression.

2.2 Physicochemical characterisation of SAHA Pluronic F-127 nanoparticles.

Pluronic® F-127 (NP) polymer nanoparticles were fabricated using thin-film hydration [46] and HA conjugated by the introduction of a disulphide pyridyl moiety (SAHA-NP-S-S) followed by HA-thiol treatment to obtain HA-coated F127 NPs (NP-HA) forming a disulphide linkage. SAHA payloads were incorporated into the micelles by co-dissolution prior to thin-film formation. Empty NPs, SAHA loaded NPs (SAHA-NP) and SAHA loaded NPs with HA conjugation (SAHA-NP-HA) were characterized using AFM peak-force tapping mode imaging [52–54] to measure morphological parameters in liquid at 37˚C (Fig. 3).

In line with reported critical micellar concentration calculations, F-127 morphological characterisation demonstrated an intact, clear spherical nature, with a measured particle diameter of ~ 40 nm and ~ 75 nm for SAHA-NP and SAHA-NP-HA respectively (Fig. 3a,b). Further F127 sample analysis was conducted to validate the AFM data using DLS. After drug incorporation, self-assembled Pluronic® F-127 micelles (NP) had diameters of 35.7 ± 3.6 nm in aqueous solution compared to 22.9 ± 20.0 nm in the no drug control (see Table 1). Both particle samples displayed uniformity, as shown in the PDI measurements, where drug loaded, SAHA-NP F-127, particles exhibited a PDI of 0.354 and the empty NP 0.243.

Table 1

((**Characterisation summary of the different Nanodelivery systems studied.** Four different nanoparticle formulations were analyzed by size, polydispersity index (PDI), zeta potential, encapsulation efficiency (EE%) and drug release profile data. *All data shown is average and standard deviation, from a minimum of three independent biological repeats.))

	Size-average (nm)	PDI	Zeta potential (mV)	Encapsulation efficiency (EE%)	Drug release maxima (h)	First order rate constant
Empty NP	22.9 ± 2.0	0.243	0.120 ± 0.25	-	-	-
SAHA-NP	35.7 ± 3.6	0.354	-0.197 ± 0.15	18%	2	2.5 +/- 0.2
SAHA-NP-S-S-	179.9 ± 15.0	0.229	-3.12 ± 0.61	42%	0.5	-
SAHA-NP-HA	251.6 ± 22.0	0.312	-14.23 ± 3.29	45%	23.5	0.3 +/- 0.03

Hyaluronic Acid (HA) is a naturally occurring polymer that consists of N-acetyl-d-glucosamine and d-glucuronic acid repeat units and is a ligand for the CD44 receptor [55]. Previously, HA-pluronic F-127 conjugates have been used to form macromolecular hydrogels, for slow drug release implants, however, there has been no application of HA-pluronic as discrete nano micelles for drug delivery [56, 57]. HA was conjugated to F-127 polymer by the introduction of a disulphide bridge by activating the PEG-diols with 4-nitrochloroformate followed by reacting with 2-(2-pyridyldithio) ethylamine to obtain NP-S-S. The efficiency of pyridyl functionalization was found to be 78% as estimated by measuring the thiopyridyl absorbance (343 nm, molar extinction coefficient of 8060 $cm^{-1}M^{-1}$) after DTT treatment. Separately, HA-thiols were synthesized by conjugating 3,3'-dithiobis (propanoic hydrazide) followed by reduction with DTT. The degree of thiol modification was estimated by Ellman's assay and was found to be 7% (with respect to the disaccharide repeat units).

Following drug incorporation, SAHA-NP-S-S displayed a hydrodynamic size of 179.9 ± 15.0 nm (Table 1), which increased to 251.6 ± 22.0 nm upon HA coating (SAHA-NP-HA). The HA coating on SAHA-NP-S-S was clearly evident from the significant decrease in zeta potential as observed for the NP-HA (-14.23 ± 3.29 mV) compared to either SAHA-NP or SAHA-NP-S-S control (-0.197 ± 0.15 mV and − 3.12 ± 0.61 mV respectively; $p < 0.05$). SAHA encapsulation efficiency was 45% for both SAHA-NP-HA and SAHA-NP-S-S (Table 1), a 2.5-fold greater encapsulation compared to SAHA-NP used above ($p < 0.05$).

Drug release at physiological salt concentrations (151.5 mM PBS; Fig. 3f) determined a delayed release between SAHA-NP and SAHA-NP-HA of approximately 15 h. The drug release maxima, the time point at which the highest concentration of SAHA release was observed, was at 2 h for SAHA-NP and 24.5 h for SAHA-NP-HA. This represents a lag of 21.5 h in maximum dose delivery following HA conjugation. The slow and sustained release of SAHA clearly demonstrates the advantage of nano formulation in terms of the efficient stabilisation of hydrophobic SAHA at the PPO core. Drug release modelling of SAHA-NP and

SAHA-NP-HA gave first-order release constants of 2.5+/-0.2 and 0.3/-0.03, indicating the addition of HA to the surface alters the release kinetics. It is likely that the slower release rates observed were due in part to the super-saturation of hydrophobic SAHA at the higher concentrations encapsulated in these particles [58]. In addition, HA is a relatively large polymer and creates a rate-limiting barrier [59, 60] resulting in increased SAHA stability in free circulation and prolonged release.

2.2.1 Pluronic F-127 stability and cellular uptake.

Pluronic® F-127 (NP) *in vitro* stability and cellular uptake is demonstrated using high content analysis using the automated multiple field of view capabilities of the In Cell 2000 microscope (**Figure S2**) [61]. Briefly Ishikawa cells were grown in the presence of F-127 particles with encapsulated propidium iodide (PI), with PI mediated fluorescence only observed following cellular internalisation, distinguishing between internalized and adsorbed nanoparticles [62]. Akin to an adherent tumour cell FACS analysis, the In Cell 2000 enabled the analysis of a minimum of 1×10^5 cells/condition, while bypassing the need to disrupt the adherent tumour cell model.[61,63] Propidium iodide fluorescence was observed in 22% NP treated cells; a four-fold increase in frequency of fluorescence compared to propidium iodide alone (5%) (**Figure S2c)**, demonstrating NP internalisation and retention.

2.3 2D In vitro cytotoxicity of SAHA nanoparticles

In order to demonstrate F-127 biocompatibility, Ishikawa cells were grown in the presence of empty NP for a period of 96 h, at a concentration of (2.5 μM). Empty F-127 NP and F-127 NP-HA particles demonstrated no significant increase in cellular toxicity when compared to the culture media only, untreated controls (Fig. 4; $p > 0.05$). Consistent with published studies, F-127 Pluronic is therefore biocompatible at low doses, in the presence and absence of the HA targeting moiety [64, 65]. Significantly reduced viability was observed in the free drug SAHA positive control group.

SAHA, NP-SAHA and SAHA-NP-HA cytotoxic effect was monitored in Ishikawa cells (see Fig. 4**).** SAHA-NP and SAHA-NP-HA resulted in significant 94% ($p < 0.05$) and 97% ($p < 0.05$) reduced Ishikawa viability after 48 h, whereas SAHA alone resulted in a smaller reduction of 41% (Fig. 4a). HA conjugation did not result in increased cytotoxicity in Hec50 cell cultures in 2D after 72 h. In Hec50 cellular viability was reduced by 79% ($p < 0.05$) at 48 h following SAHA-NP exposure, compared to a reduction of 23% in the free drug treated cells (Fig. 4b). Cell viability was further decreased after 72 h, significantly lowered by 86% ($p < 0.05$) with SAHA-NP treatment compared to 30% with SAHA free drug.

This data clearly demonstrates the substantially improved efficacy of SAHA following encapsulation. Despite the high levels of expression of CD44 observed in Hec50 cells, SAHA-NP-HA does not enhance the efficacy of the SAHA-NP in 2D cell models. This is likely due to applying the SAHA-NP directly to the surface of all cells in a 2D culture model, negating the requirement for cellular targeting, determining the need for more complex, physiologically relevant 3D culture models as well as mechanism of action investigations, investigating that this effect is not due to any alteration in drug activity following encapsulation.

2.3.1 SAHA-NP treatment alters p21 and p53 locus specific histone H3 acetylation

SAHA inhibits histone deacetylation resulting in increased histone (H3 and H4) acetylation levels [23]. SAHA has been shown to affect Ishikawa and Hec50 cell cycle progression through restoration of p21 expression [24]. Similarly SAHA treatment results in the reduction of p53 expression in type I Ishikawa cells [66, 67]. To determine that SAHA encapsulation modifies the delivery rather than the mechanism of action, global levels of acetylated histone H3 (AcH3) were compared to total H3 protein levels (See **Figure S3 a-e**). SAHA-NP resulted in 2-fold and 3-fold increases in the level of AcH3 compared to the free drug control in Ishikawa and Hec50 cells respectively. This was reflected in acH3 patterns at the p21 and p53 gene loci (see Supplementary information).

In 2D Ishikawa cells, p53 protein expression was reduced after treatment with all SAHA-NPs (Fig. 5**)**, Hec50 are p53 null, as such expression cannot be monitored. Conversely, p21 expression increased in both cell lines in response to SAHA-NP treatments, with expression levels increasing approximately four times more in Hec50 compared to Ishikawa, indicating a hyper-reactivation of p21 in these cells (Fig. 5e**)**. N-Cadherin expression following all SAHA treatments was upregulated to various degrees, while E-Cadherin was downregulated or undetectable following all SAHA treatments in both Ishikawa and Hec50, suggesting the consolidation of a more mesenchymal phenotype in the remaining viable cells.

2.4 3D In vitro cytotoxicity of SAHA nanoparticles

Whilst encapsulation clearly enhanced the efficacy of SAHA in 2D cell culture systems, the efficacy in a 3D cellular system, more closely resembling the compacted and multi-layered architecture of a solid tumour micro-environment, has yet to be reported. Such models consider the effects of complex cell-cell interactions as well as presenting nutrient and oxygen gradients [68], allowing a more physiologically relevant evaluation of the drug cytotoxicity [69]. Spheroid cultures for both Ishikawa and Hec50 were optimized (see information and **Figure S4**) prior to use as a 3-D culture model to monitor SAHA-NP efficacy and mechanism of action.

Ishikawa spheroids (Fig. 6a**)** treated with SAHA-NP showed a 75% reduction in cellular viability compared to the untreated control (Fig. 5b ($p < 0.01$), a 3.2-fold greater impact on Ishikawa cellular viability when compared directly to free drug SAHA ($p < 0.05$). Similarly, Hec50 spheroids treated with SAHA-NP showed a 40% reduction in cell viability when compared to the untreated control ($p < 0.05$), a 4-fold greater impact on Hec50 cell viability when compared to the free drug SAHA only (Fig. 6c).

SAHA-NP-HA seemingly showed an increased cytotoxic effect in both Ishikawa and Hec50 spheroids. Ishikawa cultures exhibited significant 75% reduction in cell viability following 48 h SAHA-NP treatment ($p < 0.01$) and 86% reduction with 48 h SAHA-NP-HA ($p < 0.0001$) (Fig. 6a). Hec50 3D culture viability was significantly reduced by 40% after 48 h SAHA-NP treatment for SAHA ($p < 0.05$) and 45% following exposure to SAHA-NP-HA ($p < 0.05$; (Fig. 6c). As there is a 21.5 h lag in peak SAHA release from the SAHA-NP-HA compared to SAHA-NP, we then compared the cellular cytotoxicity of both particles after 72 h. A

significantly greater cytotoxicity was observed in Ishikawa cells following 72 h ($p < 0.001$), while Hec50 cell viability was reduced further, where 58% reduction in cell viability observed after 72 h (Fig. 8d; $p < 0.01$). While surprising, Ishikawa cells exhibit a greater RFU per cell than the Hec50 population, indicating that single cell expression may be an important factor in cellular targeting, as well as the overall population fluorescence, making high content imaging a crucial consideration when developing future targeting strategies [70].

2.4.1 Spheroid Morphology and Mechanism of Action

Adopting a spheroid model can provide information such as spheroid assembly and morphology, that is not directly available with a standard 2D approach [71]. Spheroid image (Fig. 5a and d) analysis was performed using bright-field images in Image J, with an automatic mask alignment. The object area, circularity and density were the most informative metrics and used here as broad indicators of spheroid morphology, proliferation and health. Figure 6 contains the gross spheroid morphology assessment following treatment with both SAHA-NP and SAHA-NP-HA compared to free drug SAHA (using spheroid images depicted **in** Fig. 5b **and D**)

SAHA-NP treatment led to 15%, 20% and 4% reductions in Ishikawa spheroid area, circularity and density respectively compared to free drug SAHA treated samples (Fig. 7c **and Figure S5a**). Resultant Ishikawa spheroid morphological analysis at 72 h treatment (Fig. 7c**)**, demonstrated gross differences consistent to those shown at 48 h, with SAHA-NP-HA treatment resulting in a 15% reduction of spheroid area compared to the SAHA-NP, a total reduction of 30% compared to the untreated control. Minor decreases in both circularity and density were observed following SAHA-NP-HA treatments, consistent with SAHA-NP treatments, at both 48 and 72 h. The high cell specific CD44 expression observed in Ishikawa population Incell analysis, may result in an increased SAHA-NP-HA penetration into the dense Ishikawa spheroid with resultant cytotoxicity observed at 72 h consistent with the delayed SAHA release.

Hec50 spheroids are less dense, with a lower overall RFU/cell for CD44. Even greater reductions of 30%, 35% and 26% were observed in Hec50 spheroid area, circularity and density following treatment with SAHA-NP (Fig. 7f, **figure S5b).** Morphology analysis showed a drastic 80% reduction in area following SAHA-NP-HA treatments at 48 h, compared to a smaller, 20% reduction observed in the SAHA-NP sample. No change in circularity and density measures were observed. Contrastingly, 72 h SAHA-NP-HA treatments resulted in 53% and 52% reduction in spheroid circularity and density respectively, despite the observation that the total spheroid areas seem to recover. Taken alongside the cytotoxicity data, these results suggest that HA conjugation, consistent to that observed in other cancers, may lead to increased spheroid penetration and subsequent disaggregation in type II Hec50 cells [72, 73].

Loss of Hec50 sphericity was accompanied by cellular branching away from the bulk cellular mass, consistent with spheroid disaggregation. This disaggregation may be linked to increased acH3 at the p21 locus (**Figure S3d**) and resultant p21 protein expression (Fig. 7d), consistent with destabilization of integrin dimers, a crucial spheroid aggregation protein by the phosphorylation of FHL2 and translocation

to the nucleus to promote p21 expression [74, 75]. NP encapsulation therefore clearly resulted in increased SAHA efficacy, both in terms of cellular cytotoxicity and spheroid morphology in both endometrial cancer cell types. This is likely due to the altered drug release kinetics as a result of encapsulation, providing increased drug exposure over the assessed time frame, as shown by the increased levels of acH3 observed at the selected gene loci.

In addition to 3D cytotoxic and morphological analysis, we performed protein level analysis for cell cycle progression in both Ishikawa and Hec50 spheroids, to confirm consistent drug mechanism of action in 3D. As shown in 2D, p53 expression in 3D Ishikawa cells was decreased following treatment. 3D Ishikawa cultures however, in contrast to the 2D scenario (Fig. 5b), exhibited 0.34-fold and 0.56-fold reductions in p21 protein expression following treatment with SAHA-NP and SAHA-NP-HA respectively (Fig. 7a and **Figure S6)**. In p53 null Hec50 spheroids, p21 expression was upregulated with all SAHA treatments (Fig. 7d**)**, confirming a consistent effect with the 2D model. Many other studies have shown SAHA induction of p21 in a wide number of cancer cell types, resulting in cell cycle arrest [22, 77, 78]. Despite inconsistent p21 expression profiles, the significant cytotoxicity observed in 3D Ishikawa samples may indicate p21 independent cell death such as that previously observed with TRAIL mediated apoptosis [79].

EMT status has also been shown to be an important prognostic impact marker in endometrial cancer [76]. While monitoring E-cadherin and N-cadherin in these cellular systems is indicative of EMT, hypothesis can also be drawn with regard the efficacy and potential re-purposing of broad spectrum epigenetic inhibitors. HDAC inhibitors such as SAHA have been shown to induce a pro-migration phenotype [80–82]. Other studies [83] have also shown that in some instances HDACis may promote tumour aggressiveness through increasing N-cadherin [84] and decreasing of E-cadherins expression. Indeed, Ishikawa cells have been shown to undergo EMT in the presence of SAHA, as evidenced by up-regulation of N-cadherin and concomitant down-regulation of E-cadherin [67].

When HA is conjugated, potentially increasing Ishikawa spheroid penetration, the spheroid viability is reduced to almost zero, further supporting the role for nano-encapsulation of these broad-spectrum drugs. In Hec50 cells that do not express E-cadherin [80, 85], contrasting with the 2-D culture, N-cadherin remains stable after 72 h treatment with SAHA-NP-HA, suggesting no dramatic shift in EMT associated cancer motility. There was no significant change in 3D Hec50 expression of N-Cadherin following nano formulation treatments, however, N-Cadherin was increased to 1.74-fold with free drug SAHA ($p > 0.05$; Fig. 7e). This together with the spheroid morphological analysis, where clear disaggregation is accompanied by loss of circularity and density, suggest positive anti-cancer effects concomitant with significant increases in p21 expression ($p < 0.01$; **Fig. 8d**).

3. Conclusion

SAHA has been rejected as unsuitable as a single agent regime for the treatment of endometrial cancers. Although there is the negative effect on viability, by stimulating EMT there is a rational concern for the

occurrence of a refractory cancer emerging following treatment. Here we demonstrate the utility of HDACi drug encapsulation using an FDA approved nanoscale polymeric vector system, demonstrating promising results associated with spheroid penetration, suppression in cell growth, changes in P21 and P53 expression leading to a cell cycle arrest and EMT. Maintenance of polymer micelle formation stability in culture media was visualized and quantified using high content analysis. Encapsulation stabilized the SAHA activity for longer treatment periods. Equal doses of SAHA were used throughout this study and the incorporation of the drug into the NP led to a greater decrease in cellular viability in both 2D and 3D.

Many other cancers have been the focus of targeted nanoparticle treatments, with minimal studies developing targeted therapeutics for endometrial cancer. The single targeting-agent augmented nanoparticle for endometrial cancer application uses folate, despite the fact that folate receptor levels in malignant endometrial tissue is equal to or lower that of healthy tissues such as lungs and kidneys. As such, this is the first study to report a true endometrial cancer targeting nanovector for enhanced drug delivery. HA conjugation seemingly improved SAHA efficacy in more aggressive type II cell 3D spheroids, demonstrating the utility of their inclusion in preclinical evaluation pipelines for nano enhanced drug formulations. Without the inclusion of the 3-D setting here, this targeting improvement may have been dismissed following initial 2D assessments.

Recent developments in the field of HDAC inhibitors have provided new understanding of the potential applications in the treatment of solid tumour cancers. Similarly, an explosion of understanding around the role of DNA methylation and acetylation in normal and diseased cells, both in tumorigenesis and metastatic progression have led to the development of next generation drug compounds that target these mechanisms. Together, the study clearly demonstrates that epigenetic drug nanoparticle encapsulation and targeting may offer a solution to overcoming the toxicity and side effects issues observed in clinical trials. Given the demonstrated involvement of epigenetic processes in endometrial cancer this study is an important initial step into the use of this class of anti-cancerous agents for the treatment of solid tumours.

4. Methods

Hyaluronic acid (MW 130 kDa) was purchased from LifeCore Biomedical (Chaska, USA). 1-ethyl-3-(3-dimethylaminopropyl)-carbodiimide hydrochloride (EDC), 1-hydroxybenzotriazole hydrate (HOBt), DL-Dithiothreitol (DTT), Cysteamine hydrochloride, 2,2'-Dithiodipyridine, 4-Nitrophenyl chloroformate were purchased from Sigma-Aldrich. Dialysis membranes used for purification were purchased from Spectra Por-6 (MWCO 3500). All solvents were of analytical quality. Nuclear Magnetic Resonance (NMR) spectroscopy experiments were performed with a Varian Mercury 300 MHz NMR Spectrometer (Palo Alto, USA). All spectrophotometric analysis was carried out on Shimadzu UV-3600 plus UV-VIS-NIR spectrophotometer.

2D Cell culture

Both Ishikawa (ECACC 99040201 Public Health England, UK) a type I endometrial cancer (TIEC) model and Hec-50B (Cat-No 1145, JCRB Cell Bank, Japan) a type II endometrial cancer (TIIEC) model [49], were maintained in DMEM:F-12 (1:1) + GlutaMax™ full media (Cat-No 31331-028, Gibco, ThermoFisher Scientific, UK) supplemented with 10% foetal bovine serum (FBS), sodium bicarbonate 1 mM, sodium pyruvate 1 mM and 1% antibiotic-antimycotic solution in plastic culture flasks at 37 °C and 5% CO_2 incubator (Nuaire). Cells were supplemented with full serum media every 2 days and passaged when confluent.

3D cell culture

Spheroids were prepared for viability experiments using an ultra-low attachment 96 well plate [86]. 4×10^3 cells per well were added to a 96-well Ultra-Low Attachment surface (ULA) microplate (Corning™ 4520) supplemented with stripped serum media. After 48 h treatment incubation, CellTiter-Glo® 3D Cell Viability Assay reagents (Promega) were added following manufacturer's instructions and luminescence recorded using a microplate reader (FLUOstar Omega) at RT. Spheroids for protein expression were prepared using the liquid overlay technique in clear 96 well plates [87]. Briefly, 96 well plates were conditioned for spheroid seeding by coating the bottom of each well with 2% agarose. The agarose was left to set for 1 h in the flow hood under ultraviolet (UV) light to ensure sterility. 6×10^4 cells/mL were used to form the spheroids for western blot experiments. Spheroid morphology following treatments was assessed using Image J (FIJI). Images were taken using a Zeiss microscope at 40X objective with scale bar exported from the proprietary Zen software (Carl Zeiss Ltd, UK). Scale bar consistent exported images were analyzed in Image J (FijiLOCI, University of Wisconsin, USA), setting measurements to include area, perimeter and shape descriptors using the particle analyzer function.

Synthesis of thiolated HA (HA-SH)

HA-SH conjugates were synthesized by coupling dithiobis (propanoic hydrazide) (DTPH) using carbodiimide chemistry to the carboxylic groups of HA and subsequently reducing the disulphide bond using dithiothreitol (DTT). Briefly, 1 equivalent HA (400 mg, 1 mmol with respect to the disaccharide repeat units) was dissolved in 120 ml of deionized water followed by the addition of 1 equivalent 3,3'-dithiobis (propanoic hydrazide) (DTPH 238.3 mg, 1 mmol) and 1 equivalent HOBt (153 mg, 1 mmol) and stirred at room temperature until the reaction becomes homogeneous. Thereafter, the pH of the reaction mixture was adjusted to 4.7 by careful addition of 1 M NaOH and 1 M HCl. Finally, 0.25 mmol EDC·HCl (48 mg, 0.25 equivalent) was added and allowed to stir overnight. Then the reaction mixture was loaded into a dialysis bag (Spectra Por-6, MWCO 3500 g/ mol) and dialyzed against dilute HCl (pH = 3.5) containing 100 mM NaCl (4 × 2L, 48 h) and then dialyzed against deionized water (2 × 2L, 24 h). The solution was lyophilized to obtained as white fluffy material. The degree of hydrazide modification was estimated to be 10.5% (with respect to the disaccharide repeat units) as determined by trinitrobenzene sulfonic acid (TNBS) assay by measuring absorbance at 500 nm, using UV spectroscopy [88].

In the second step, the lyophilized HA-DTPH derivative was dissolved in 100 ml deionized water and pH of the solution was adjusted to 9 with 1 M NaOH. Subsequently, dl-Dithiothreitol (DTT, 124 mg, 0.8 mmol) was added dropwise to the solution. The mixture was stirred overnight, after which the solution was transferred to a dialysis bag (Spectra Por-6, MWCO 3500 g/ mol) and dialyzed against deionized water (3 × 2L, 24 h). The dialyzed solution was lyophilized to give white fluffy thiol-modified HA (HA-SH). The concentration of thiol groups was estimated to be 7% (with respect to the disaccharide unit) by Ellman's assay using the extinction coefficient of 14 150 $M^{-1}cm^{-1}$ at 412 nm using UV spectroscopy [89].

Synthesis of thiol-terminated Pluronic® F-127 (NP-S-S-Py)

Activation of Pluronic F127

The synthesis of pluronic F127 functionalized with terminal disulphide pyridyl was performed following the reported procedure [90]. Briefly, the terminal PEG diols of pluronic F127 was activated using 4-nitrochloroformate. The degree of activation was found to be 78%, determined spectrophotometrically by measuring the amounts of 4-nitrophenolate ions released in the alkaline solution by measuring the absorbance at 402 nm using a molar extinction coefficient of 18400 $cm^{-1}M^{-1}$.

Synthesis of pyridyl disulphide ligand (2-(2-pyridyldithio) ethylamine)

Cysteamine hydrochloride (2.288 gm, 20.1408 mmol) was dissolved in methanol (17.5 ml) followed by the addition of glacial acetic acid (1.6 ml). Above solution was then dropwise added to a stirred solution of 2,2-dithiopyridine (8.815 gm, 40.2817 mmol) in methanol (41.6 ml). Reaction mixture was stirred for 48 h at room temperature and product was precipitated from stirred diethyl ether (200 ml). The product was dissolved in a small volume of methanol and was again precipitated by diethyl ether to afford white solid compound. The 1H NMR of the pyridyl disulphide product was consistent with the reported data [90].

Synthesis of F127 pyridyl disulphide derivative (NP-S-S-Py)

Activated pluronic F127 (1 gm, 0.069 mmol) dissolved in 10 ml DCM was reacted with extracted disulphide ligand (154 mg, 0.69 mmol) dissolved in 1 ml DCM. The reaction mixture was refluxed overnight. It was then concentrated and diluted with methanol:water (1:1, v/v, 10 ml) and dialyzed (membrane MWCO 3500 Da) against 2 L deionized water for two days. The product was obtained as white fluffy material after lyophilization. The modification was determined using UV (343 nm, molar extinction coefficient of 8060 $cm^{-1}M^{-1}$). The UV absorbance of product (1 mg/ml in PBS buffer at pH 9) was measured before as well as 10 min after the addition of 0.1 ml of DTT (15 mg/1000 ml in PBS at pH 9). The percentage modification was found to be 78%.

Pluronic micelle fabrication

Pluronic® F-127 (NP) and thiol-terminated Pluronic® F-127 (NP-S-S) micelles were fabricated using thin-film hydration method described by Caldwell et al.[91] The polymer constituent and 10% SAHA (Cayman

Chemical Company, 10009929) / propidium iodide (Sigma-Aldrich, P4170-10MG) were dissolved in acetonitrile (ACN). The acetonitrile was removed by rotary evaporation at 65 °C and under 226 mbar for 1 h, and the flask placed into a desiccator under vacuum overnight, to ensure the film was void of all moisture and residual copolymer matrix acetonitrile removed. Prior to hydration, samples were heated to 65 °C in a water bath under mild rotation for 1 h until the sample resembled a viscous thin film coating the flask. NPs were hydrated in deionized water and returned to heated rotation for 30 min to ensure maximum micelle formation and drug loading. HA-thiol was added in excess (2:1) to NP-S-S and mixed using a magnetic stirrer at 700 rpm for 1 h to form NP-HA; prior to use HA-thiol was sterilized under UV for 1 h. An 0.22 µm filter (Millipore) was applied on all samples – except NP-HA samples – to remove non-encapsulated drugs agglomeration.

Size and Zeta potential analysis with dynamic light scattering

Polymeric micelle size and zeta potential were determined using Zetasizer Nano ZS™ (Malvern, UK), at a concentration of 100 µg/ml. A series of data indicating size, zeta- average, polydispersity index was generated. All data is presented as average and standard deviation, from a minimum of three independent biological repeats.

Atomic Force Microscope (AFM)

10 µL nanoparticle aliquots were spotted on mica substrates at a concentration of 100 µg/mL (AGG250-1, Agar Scientific, UK) and dried at RT. Sample topography was obtained in air using a Bruker BioScope Catalyst (Bruker Instruments, Santa Barbara, California, USA) AFM. Bruker ScanAsyst-Air cantilevers were used, with a nominal spring constant of 0.4 N/m and a nominal resonant frequency of 70 kHz. All imaging was conducted using Peak Force Tapping (PFT) in ScanAsyst Mode. Images were processed with first-order flattening and planefit using Bruker Nanoscope Analysis 1.5, the height of the particles was calculated using freeware AFM software WsXM 5.0 [92].

HPLC-UV quantification

An Agilent detector equipped with autosampler and a C18 reversed-phase column (Xbridge C18, 130 Å, 3.5 µm, 2.1 mm x150 mm) was ran isocratically at room temperature (RT). All samples were diluted using acetonitrile and loaded into the 0.3 mL polypropylene, 9 mm thread, screw thread vials (Sigma, 29377-U); mobile phase throughout analysis was 0.1% formic acid:acetonitrile 78:22.[93] A flow rate of 0.25 µL/min and sample injection volume of 2 µL gave a 7 min analyte retention time. Following elution from the column, the sample was run through the UV/vis detector recording at 241 nm. Nanoparticle samples were diluted 1:10, 1:100 and 1:200 to ensure measurements were occurring within the range of the standard curve. Encapsulation efficiency was determined using the equation below (1).

$$Encapsulation\ Efficiency\ (EE\%) = \frac{mass\ of\ drug\ in\ particles}{mass\ of\ drug\ used\ in\ fabrication} x100 \qquad (1)$$

Drug release profile

Cellulose dialysis sacks with a molecular weight cut-off pore size of 12 kDa (Sigma Aldrich, D6191-25EA) were used to monitor drug release profiles over 80 h. Dialysis sacks were soaked in PBS buffer overnight, 1.5 mL of sample was loaded into the cellulose tubing and placed in a beaker containing 20 mL of PBS and a small magnetic fly. The buffer was mixed continually throughout the experiment by stirring at 300 rpm. For the first 2 h of dialysis, 1 mL samples were taken at 30 min intervals, for the remainder of the first 48 h samples were taken every 60 min. Following each sampling, 1 mL of fresh PBS was reintroduced to maintain a total volume of 20 mL. Samples were diluted in ACN to dissociate polymer micelles and frozen until analysis.

2D / 3D Cell viability assays

Cell viability assays were performed in 2D using Realtime-Glo™ MT Cell Viability RT-Glo (Promega UK, G9711) and in 3D using Celltiter-Glo 3D (Promega UK, G9682). Both methods were performed according to the manufacturer's instructions [94, 95]. Readings were taken using a FLUOstar Omega microplate reader at 0-, 24-, 48- and 72 h time points. For 3D experiments, only 48 h and 72 h timepoint was investigated. The spectrophotometer was heated to 37 °C prior to readings. All SAHA-NP preparations were compared to free drug SAHA and all data was normalized against the control cell line without any treatment.

Protein blotting and antibodies

Total protein lysates (20 µg) were resolved on a precast 4–20% polyacrylamide gels (mini-PROTEAN® TGX stain-free™ gels, 456–8094), transferred and immobilized onto polyvinylidene fluoride (PVDF) membranes (mini format Trans-Blot® Turbo™ transfer pack, 170–4156), incubated for 60 min at room temperature in blocking solution (TRIS-buffered saline containing 5% BSA and 0.1% Tween 20), followed by an overnight incubation in primary antibodies at 4 °C at 1:1000 dilution. The following antibodies were used: Cell Signalling (Danvers, MA): p21 (#2947s; 1:1000), p53 (#9282s; 1:1000), Santa Cruz: GAPDH (# sc-47724; 1:1000). Abcam (Cambridge, MA): E-Cadherin (#1416; 1:1000), N-Cadherin (#18203; 1:1000), GE Healthcare Lifescience: Anti-Rabbit (#10794347, 1:2000), Anti-Mouse (#10094724, 1:2000). Membranes were then washed three times and incubated with horseradish peroxidase–conjugated secondary antibodies for 1 h at 1:2000 dilution.

Statistical Analysis

Data were normalized against the respective cell line without any treatment. Statistical analyses used to in this study to validate results, unless stated otherwise, were pairwise student's T-Tests and ANOVA where treatments were compared against the free drug only. Significance is indicated on graphs or tables, when appropriate in the following fashion: $p \leq 0.05$ denoted by *, $p \leq 0.01$ by **, $p \leq 0.001$ by *** and $p \leq 0.0001$ by ****.

Declarations

Ethics approval and consent to participate

Not applicable

Consent for publication

Not applicable

Availability of data and materials

The datasets used and/or analysed during the current study are available from the corresponding author on reasonable request.

Competing interests

The authors declare that they have no competing interests.

Funding

The authors wish to thank the KESS II scheme for supporting Kadie Edwards with this research and co-funding provided by the Welsh Government's European Social Fund (ESF) convergence programme for West Wales and the Valleys. We thank the Celtic Advanced Life Science Innovation Network (CALIN) for supporting Dr Seydou Yao. We wish to thank the Erasmus + Mobility Scheme for supporting both Simone Pisano and Veronica Feltraccao, this project was co-funded by the European Union. We thank Life Sciences Research Network Wales: project grant 'Nanoparticle delivery of epigenetic modifiers: a targeted approach for Endometrial Cancer treatment' for supporting the work of Dr Katja Brusehafer. The authors thank the Natural and Environmental Research Council, UK [grant number NE/K004212/1] and SMARTExpertise 2014–2020 West Wales and the Valleys, European Regional Development Fund, under Grant 2017/COL/001 for supporting the work of Dr Andrea Gazze.

Author's contributions

KE contributed data acquisition, analysis, interpretation and manuscript drafting; **SY** study design and conception, data acquisition and manuscript drafting; **SP** study design, data acquisition and interpretation; **VF** data acquisition; **KB** data acquisition, analysis and interpretation; **SS and OPO** conducted synthesis of thiol-terminated Pluronic® F-127 and thiolated HA. **AG, HM, CL** data acquisition, analysis and interpretation and provided expertise in NP fabrication; **DG** contributed to project conception and design; **RSC** project conception, design and involved in manuscript drafting; **LWF** project conception,

design, oversight of experiments, data interpretation, manuscript revision and final approval. All authors read and approved the final manuscript.

References

1. Patra JK, Das G, Fraceto LF, Campos EVR, Rodriguez-Torres MdelP, Acosta-Torres LS, Diaz-Torres LA, Grillo R, Swamy MK, Sharma S, Habtemariam S, Shin H-S. J Nanobiotechnology. 2018. DOI 10.1186/s12951-018-0392-8.
2. Lortet-Tieulent J, Ferlay J, Bray F, Jemal A. J Natl Cancer Inst. 2018. DOI 10.1093/jnci/djx214.
3. NCIN. “Outline of Uterine Cancer in the United Kingdom: Incidence, Mortality and Survival,” 2013.
4. Bray F, Ferlay J, Soerjomataram I, Siegel RL, Torre LA, Jemal A. CA CANCER J CLIN 2018, 0, DOI 10.3322/caac.21492.
5. cancer research UK. “Uterine cancer statistics,” 2016.
6. Morice P, Leary A, Creutzberg C, Abu-Rustum N, Darai E. Lancet. 2016;387:1094.
7. 10.1136/bmj.d3954
   Saso S, Chatterjee J, Georgiou E, Ditri AM, Smith JR, Ghaem-Maghami S, *BMJ* 2011, *343*, DOI 10.1136/bmj.d3954.
8. Frei KA, Kinkel K. J Magn Reson Imaging. 2001. DOI 10.1002/jmri.1121.
9. 10.1016/j.jsbmb.2007.09.020
   Doll A, Abal M, Rigau M, Monge M, Gonzalez M, Demajo S, Colás E, Llauradó M, Alazzouzi H, Planagumá J, Lohmann MA, Garcia J, Castellvi S, JR y. Cajal, Gil-Moreno A, Xercavins J, Alameda F, Reventós J, *J. Steroid Biochem. Mol. Biol.* 2008, DOI 10.1016/j.jsbmb.2007.09.020.
10. Hoffman BL, Schorge JO, Schaffer JI, Halvorson LM, Bradshaw KD, Cunningham FG, Calver LE. *Williams Gynecol*. 2012.
11. et al. Lodish H, Berk A, Zipursky SL, *DNA Damage and Repair and Their Role in Carcinogenesis. Molecular Cell Biology. 4th Edition*, New York, 2000.
12. Vale CL, Tierney J, Bull SJ, Symonds PR. Cochrane Database Syst Rev. 2012. DOI 10.1002/14651858.CD003915.pub4.
13. Risinger JI, Maxwell GL, Chandramouli GVR, Jazaeri A, Aprelikova O, Patterson T, Berchuck A. J. C. Barrett, *Cancer Res.* 2003.
14. Nagashima M, Miwa N, Hirasawa H, Katagiri Y, Takamatsu K, Morita M. Sci Rep. 2019;9:6469.
15. 10.4161/epi.5.6.12431
   Tao MH, Freudenheim JL, *Epigenetics* 2010, DOI 10.4161/epi.5.6.12431.
16. Sakuragi N. Int J Clin Oncol. 2013. DOI 10.1007/s10147-013-0535-8.
17. 10.3109/00313025.2010.520307
   Arafa M, Somja J, Dehan P, Kridelka F, Goffin F, Boniver J, Delvenne P, *Pathology* 2010, DOI 10.3109/00313025.2010.520307.

18. 10.2217/epi-2016-0166
Bartosch C, Lopes JM, Jerónimo C, *Epigenomics* 2017, DOI 10.2217/epi-2016-0166.
19. Cancer Genome Atlas Research Network. Kandoth C, Schultz N, Cherniack AD, Akbani R, Liu Y, Shen H, Robertson AG, Pashtan I, Shen R, Benz CC, Yau C, Laird PW, Ding L, Zhang W, Mills GB, Kucherlapati R, Mardis ER, Levine DA. Nature 2013, DOI 10.1038/nature12113.
20. Lechner M, Boshoff C, Beck S. *Cancer Epigenome*, 2010.
21. Ma X, Ma CX, Wang J. Am J Mol Biol. 2014. DOI 10.4236/ajmb.2014.43015.
22. Ren J, Zhang J, Cai H, Li Y, Zhang Y, Zhang X, Zhao D, Li Z, Ma H, Wang J, Gao Y, Xiao L, Liu R, Qian J, Liu Y, Wei H, Li J. Curr Pharm Des. 2014. DOI 10.2174/13816128113199990528.
23. Jiang S, Dowdy SC, Meng XW, Wang Z, Jones MB, Podratz KC, Jiang SW. Gynecol Oncol. 2007. DOI 10.1016/j.ygyno.2007.01.012.
24. Takai N, Narahara H, Takai N, Narahara H. Curr Med Chem. 2007. DOI 10.2174/092986707782023299.
25. Fröhlich LF, Mrakovcic M, Smole C, Zatloukal K. Cancer Cell Int. 2016. DOI 10.1186/s12935-016-0343-0.
26. Nervi C, De Marinis E, Codacci-Pisanelli G. Clin Epigenetics. 2015. DOI 10.1186/s13148-015-0157-2.
27. 10.7150/thno.7193
Kobayashi H, Watanabe R, Choyke PL, *Theranostics* 2014, DOI 10.7150/thno.7193.
28. Blanco E, Shen H, Ferrari M. Nat Biotechnol. 2015;33:941.
29. Jia L. Curr Nanosci. 2005. DOI 10.2174/157341305774642939.
30. Ebeid K, Meng X, Thiel KW, Do AV, Geary SM, Morris AS, Pham EL, Wongrakpanich A, Chhonker YS, Murry DJ, Leslie KK, Salem AK. Nat Nanotechnol. 2018;13:72.
31. Wilhelm S, Tavares AJ, Dai Q, Ohta S, Audet J, Dvorak HF, Chan WCW. Nat Rev Mater. 2016. DOI 10.1038/natrevmats.2016.14.
32. 10.12688/f1000research.9690.1
Wang Y-F, Liu L, Xue X, Liang X-J, *F1000Research* 2017, DOI 10.12688/f1000research.9690.1.
33. Safra T, Muggia F, Jeffers S, Tsao-Wei DD, Groshen S, Lyass O, Henderson R, Berry G, Gabizon A. Ann Oncol. 2000. DOI 10.1023/A:1008365716693.
34. 10.1159/000381716
Clift AK, Drymousis P, Al-Nahhas A, Wasan H, Martin J, Holm S, Frilling A, *Neuroendocrinology* 2015, DOI 10.1159/000381716.
35. Minchinton AI, Tannock IF. Nat Rev Cancer. 2006. DOI 10.1038/nrc1893.
36. Heldin CH, Rubin K, Pietras K, Östman A. Nat Rev Cancer. 2004. DOI 10.1038/nrc1456.
37. Rompicharla SVK, Trivedi P, Kumari P, Ghanta P, Ghosh B, Biswas S. Nanomedicine. 2017;12:43.
38. Xu J, Sun J, Wang P, Ma X, Li S. J Drug Target. 2018;26:448.

39. Jahangirian H, Lemraski EG, Webster TJ, Rafiee-Moghaddam R, Abdollahi Y. Int J Nanomedicine. 2017;12:2957.
40. De Jong WH, Borm PJA. Int J Nanomedicine. 2008;3:133.
41. Jung HH, Park K, Han DK. J Control Release. 2010. DOI 10.1016/j.jconrel.2010.06.020.
42. Akash MSH, Rehman K, Chen S. Polym Rev. 2014. DOI 10.1080/15583724.2014.927885.
43. Diniz IMA, Chen C, Xu X, Ansari S, Zadeh HH, Marques MM, Shi S, Moshaverinia A. J Mater Sci Mater Med. 2015. DOI 10.1007/s10856-015-5493-4.
44. MIYAZAKI S, YOKOUCHI C, NAKAMURA T, HASHIGUCHI N, HOU W-M, TAKADA M. Chem Pharm Bull (Tokyo). 2011. DOI 10.1248/cpb.34.1801.
45. Wang H, Williams GR, Wu J, Wu J, Niu S, Xie X, Li S, Zhu LM. Int J Pharm. 2019;559:289.
46. Hong W, Shi H, Qiao M, Zhang Z, Yang W, Dong L, Xie F, Zhao C, Kang L. Sci Rep 2017, 7, DOI 10.1038/srep42465.
47. Afify AM, Craig S, Paulino AFG, Stern R. Ann Diagn Pathol. 2005;9:312.
48. Wojciechowski M, Krawczyk T, Śmigielski J, Malinowski A. Arch Gynecol Obstet. 2015;291:383.
49. Kozak J, Wdowiak P, Maciejewski R, Torres A. Cytotechnology. 2018;70:339.
50. Kelly WK, Marks PA. Nat Clin Pract Oncol. 2005. DOI 10.1038/ncponc0106.
51. Komatsu N, Kawamata N, Takeuchi S, Yin D, Chien W, Miller CW, Koeffler HP. *Oncol. Rep*. 2006.
52. Edwardson JM, Henderson RM. Drug Discov Today. 2004. DOI 10.1016/S1359-6446(03)02905-2.
53. Maver U, Velnar T, Gaberšček M, Planinšek O, Finšgar M. TrAC - Trends Anal Chem. 2016. DOI 10.1016/j.trac.2016.03.014.
54. *Atomic Force Microscopy in Biomedical Research*, 2011.
55. Mattheolabakis G, Milane L, Singh A, Amiji MM. J Drug Target. 2015;23:605.
56. Kim M, Hwang Y, Tae G. Int J Biol Macromol. 2016;93:1603.
57. Chen YY, Wu HC, Sun JS, Dong GC, Wang TW. Langmuir. 2013;29:3721.
58. Gref R, Torchilin V, Minamitake Y, Peracchia M, Trubetskoy V, Langer R. *Science (80-.)*. 2006, DOI 10.1126/science.8128245.
59. Dinarvand R, Sepehri N, Manoochehri S, Rouhani H, Atyabi F. Int J Nanomedicine. 2011. DOI 10.2147/IJN.S18905.
60. Gao P, Nie X, Zou M, Shi Y, Cheng G. J Antibiot (Tokyo). 2011;64:625.
61. Gomes-Alves AG, Maia AF, Cruz T, Castro H, Tomás AM. *PLoS One* 2018, DOI 10.1371/journal.pone.0201747.
62. Stiefel P, Schmidt-Emrich S, Maniura-Weber K, Ren Q. BMC Microbiol. 2015;15:36.
63. Leonard AP, Appleton KM, Luttrell LM, Peterson YK. Microsc Microanal. 2013. DOI 10.1017/S1431927612014067.
64. Li YY, Li L, Dong HQ, Cai XJ, Bin T, Ren. Mater Sci Eng C. 2013;33:2698.
65. Lee Y, Chung HJ, Yeo S, Ahn C-H, Lee H, Messersmith PB, Park TG. Soft Matter. 2010;6:977.

66. Li D, Marchenko ND, Moll UM. Cell Death Differ. 2011. DOI 10.1038/cdd.2011.71.
67. Uchida H, Maruyama T, Nishikawa-Uchida S, Oda H, Miyazaki K, Yamasaki A, Yoshimura Y. J Biol Chem. 2012. DOI 10.1074/jbc.M111.286138.
68. Lovitt C, Shelper T, Avery V. Biology (Basel). 2014. DOI 10.3390/biology3020345.
69. Nirmalanandhan VS, Duren A, Hendricks P, Vielhauer G, Sittampalam GS. Assay Drug Dev Technol. 2010. DOI 10.1089/adt.2010.0276.
70. Jeon J, Nim S, Teyra J, Datti A, Wrana JL, Sidhu SS, Moffat J, Kim PM. Genome Med. 2014;6:57.
71. Mittler F, Obeïd P, Rulina AV, Haguet V, Gidrol X, Balakirev MY. Front Oncol 2017, 7, DOI 10.3389/fonc.2017.00293.
72. Lee SY, Park JH, Ko SH, Shim JS, Kim DD, Cho HJ. ACS Appl Mater Interfaces. 2017;9:22308.
73. El-Dakdouki MH, Puré E, Huang X. Nanoscale. 2013;5:3904.
74. Nakazawa N, Sathe AR, Shivashankar GV, Sheetz MP, *Proc. Natl. Acad. Sci. U. S. A.* 2016, *113*, E6813.
75. Casey RC, Burleson KM, Skubitz KM, Pambuccian SE, Oegema TR, Ruff LE, Skubitz APN, *Am. J. Pathol.* 2001, *159*, 2071.
76. Tanaka Y, Terai Y, Kawaguchi H, Fujiwara S, Yoo S, Tsunetoh S, Takai M, Kanemura M, Tanabe A, Ohmichi M. Cancer Biol Ther. 2013;14:13.
77. Yin D, Ong JM, Hu J, Desmond JC, Kawamata N, Konda BM, Black KL, Koeffler HP. Clin Cancer Res. 2007. DOI 10.1158/1078 – 0432.CCR-06-1261.
78. 10.1073/pnas.180316197
Richon VM, Sandhoff TW, Rifkind RA, Marks PA, *Proc. Natl. Acad. Sci.* 2002, DOI 10.1073/pnas.180316197.
79. Zhou X, Liu Z, Wang H, Liu X, Zhou Z, Tang J, Liu X, Zheng M, Shen Y. J Drug Target. 2019;27:306.
80. Serrano-Gomez SJ, Maziveyi M, Alahari SK. Mol Cancer. 2016. DOI 10.1186/s12943-016-0502-x.
81. Lin HY, Chen CS, Lin SP, Weng JR, Chen CS. Med Res Rev. 2006. DOI 10.1002/med.20056.
82. Ropero S, Esteller M. Mol Oncol. 2007. DOI 10.1016/j.molonc.2007.01.001.
83. Kong D, Ahmad A, Bao B, Li Y, Banerjee S, Sarkar FH. *PLoS One* 2012, DOI 10.1371/journal.pone.0045045.
84. Nguyen HPT, Xiao L, Deane JA, Tan KS, Cousins FL, Masuda H, Sprung CN, Rosamilia A, Gargett CE. Hum Reprod. 2017. DOI 10.1093/humrep/dex289.
85. Takai N, Desmond JC, Kumagai T, Gui D, Said JW, Whittaker S, Miyakawa I, Koeffler HP. Clin Cancer Res. 2004. DOI 10.1158/1078 – 0432.CCR-03-0100.
86. Amaral RLF, Miranda M, Marcato PD, Swiech K. Front Physiol. 2017. DOI 10.3389/fphys.2017.00605.
87. Costa EC, de Melo-Diogo D, Moreira AF, Carvalho MP, Correia IJ. Biotechnol J. 2018. DOI 10.1002/biot.201700417.
88. Gurav D, Varghese OP, Hamad OA, Nilsson B, Hilborn J, Oommen OP. Chem Commun. 2016;52:966.

89. Koivusalo L, Kauppila M, Samanta S, Parihar VS, Ilmarinen T, Miettinen S, Oommen OP, Skottman H. Biomaterials 2019, 225, DOI 10.1016/j.biomaterials.2019.119516.
90. Li J-T, Carlsson J, Lin J-N, Caldwell KD. Bioconjug Chem. 1996;7:592.
91. Karin Maria Elisabet Caldwell;, Carlsson PJE-TL. *Coating of Hydrophobic Surfaces to Render Them Protein Resistant While Permitting Covalent Attachment of Specific Ligands*, 1998.
92. Horcas I, Fernández R, Gómez-Rodríguez JM, Colchero J, Gómez-Herrero J, Baro AM. Rev Sci Instrum. 2007. DOI 10.1063/1.2432410.
93. Kwak TW, Kim DH, Jeong Y-I, Kang DH. J Nanobiotechnology. 2015;13:60.
94. Idrees A, Chiono V, Ciardelli G, Shah S, Viebahn R, Zhang X, Salber J. *Int. J. Artif. Organs* 2018, DOI 10.1177/0391398818775519.
95. Duellman SJ, Zhou W, Meisenheimer P, Vidugiris G, Cali JJ, Gautam P, Wennerberg K, Vidugiriene J. Assay Drug Dev Technol. 2015;13:456.
96. Wesley Overton K, Spencer SL, Noderer WL, Meyer T, Wang CL, *Proc. Natl. Acad. Sci. U. S. A.* 2014, *111*, E4386.
97. Holmes KA, Brown GD, Carroll JS. in *Methods Mol. Biol.*, 2016.
98. Hunter AL, Narang N, Baxter M, Ray DW, Poolman TM. J Mol Endocrinol. 2019;62:169.
99. 10.3390/molecules20033898
Mottamal M, Zheng S, Huang TL, Wang G, *Molecules* 2015, DOI 10.3390/molecules20033898.

Figures

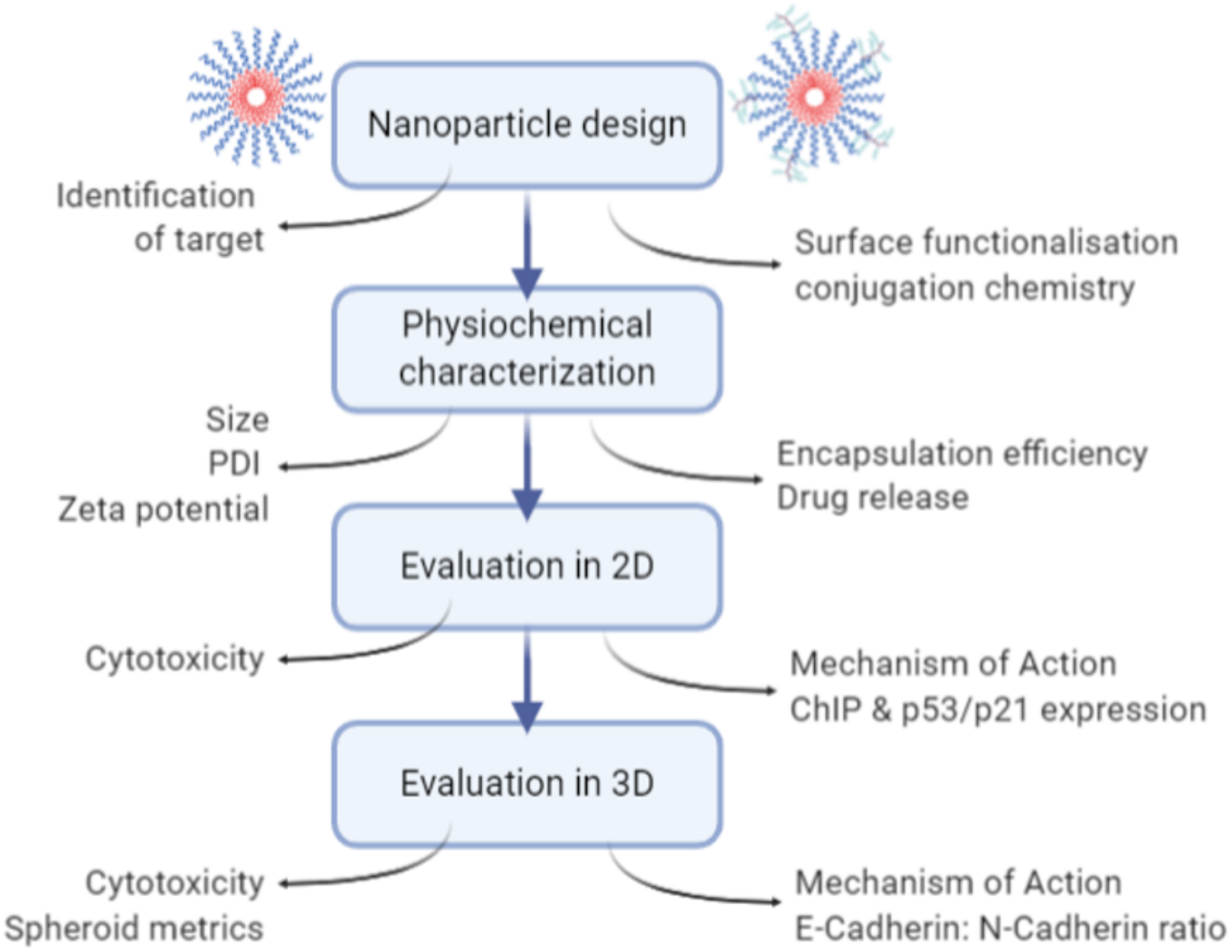

Figure 1

Experimental flow diagram.

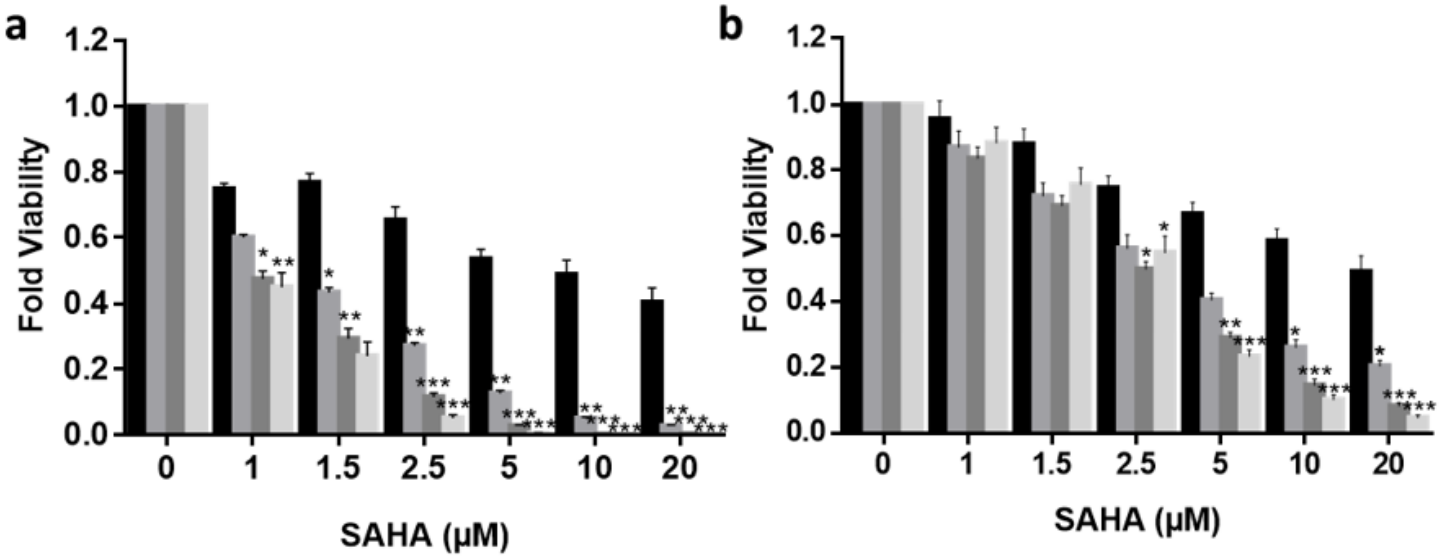

Figure 2

Free SAHA drug cytotoxicity in in vitro Endometrial cancer models. Increasing concentrations (1μM to 25μM) of free SAHA were added to both Ishikawa (a) and Hec50 (b) cells over a 96hr period and viability quantified using Real Time Glo viability test (N=3). All data was normalized to the untreated control cells.

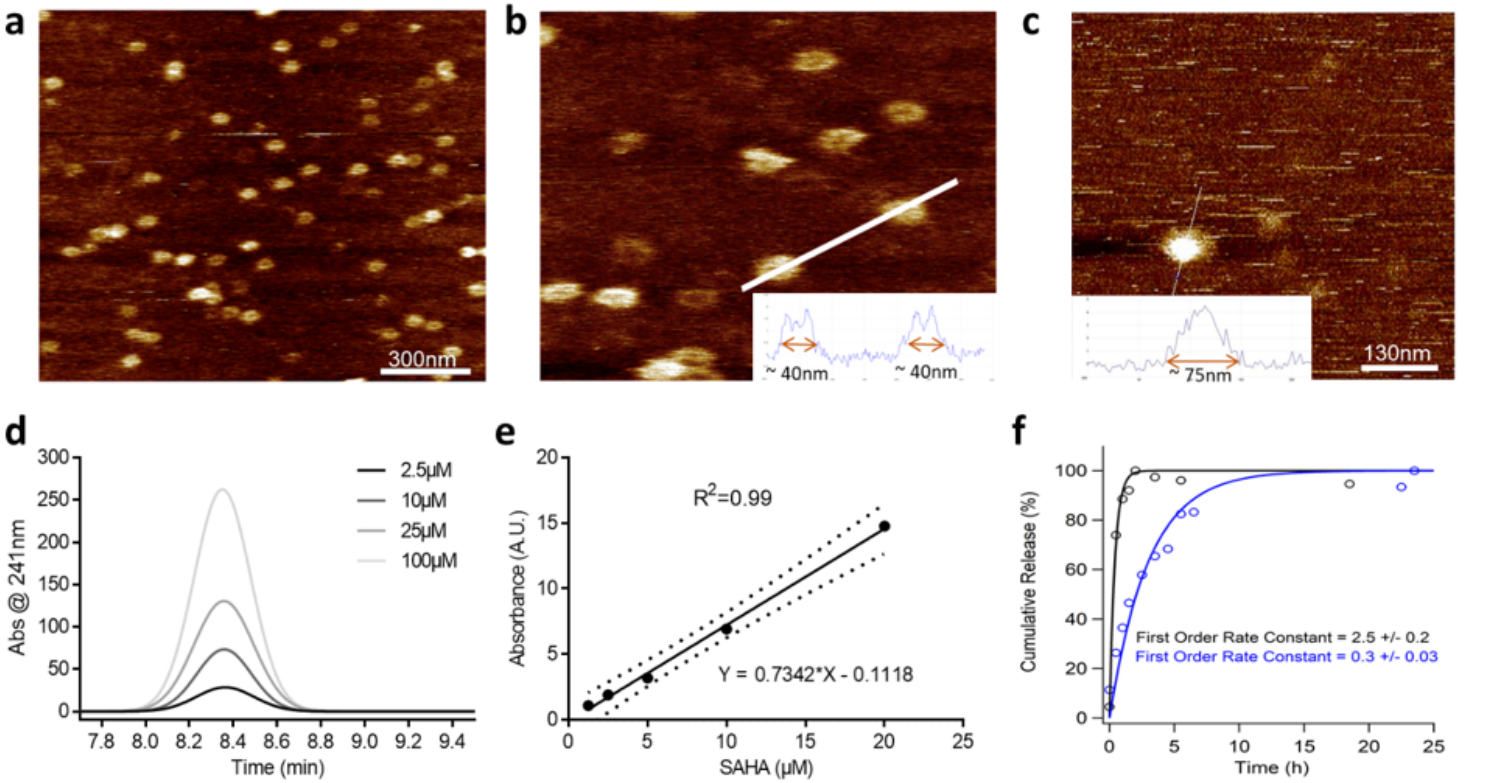

Figure 3

Nanoparticle AFM imaging. F127 nanoparticles were deposited on a mica substrate and analyzed by AFM. (a) NP topography showing the round shape. (b) Vertical line profile calculated along the solid white dotted line showing particle height around 40nm. Scale bar 300nm. (c) NP-HA image showing size and topography. Encapsulation efficiency and release profile HPLC chromatogram and calibration curve. SAHA encapsulation efficiency was calculated relative to a standard curve constructed from increasing SAHA concentrations from 2.5-100μM (absorbance at 241 nm and retention time = 8.34 mins) in DMSO solution, measured by HPLC (d). Calibration curve (e) and linear fitting are representative of that constructed independently for each particle preparation. The purity (based on AUC) was >95%. Cumulative SAHA release profiles from nanoparticles (f). Data generated using LC-UV analysis. SAHA-NP (black line) and SAHA-NP-HA (blue line) release profiles with corresponding first order rate constant.

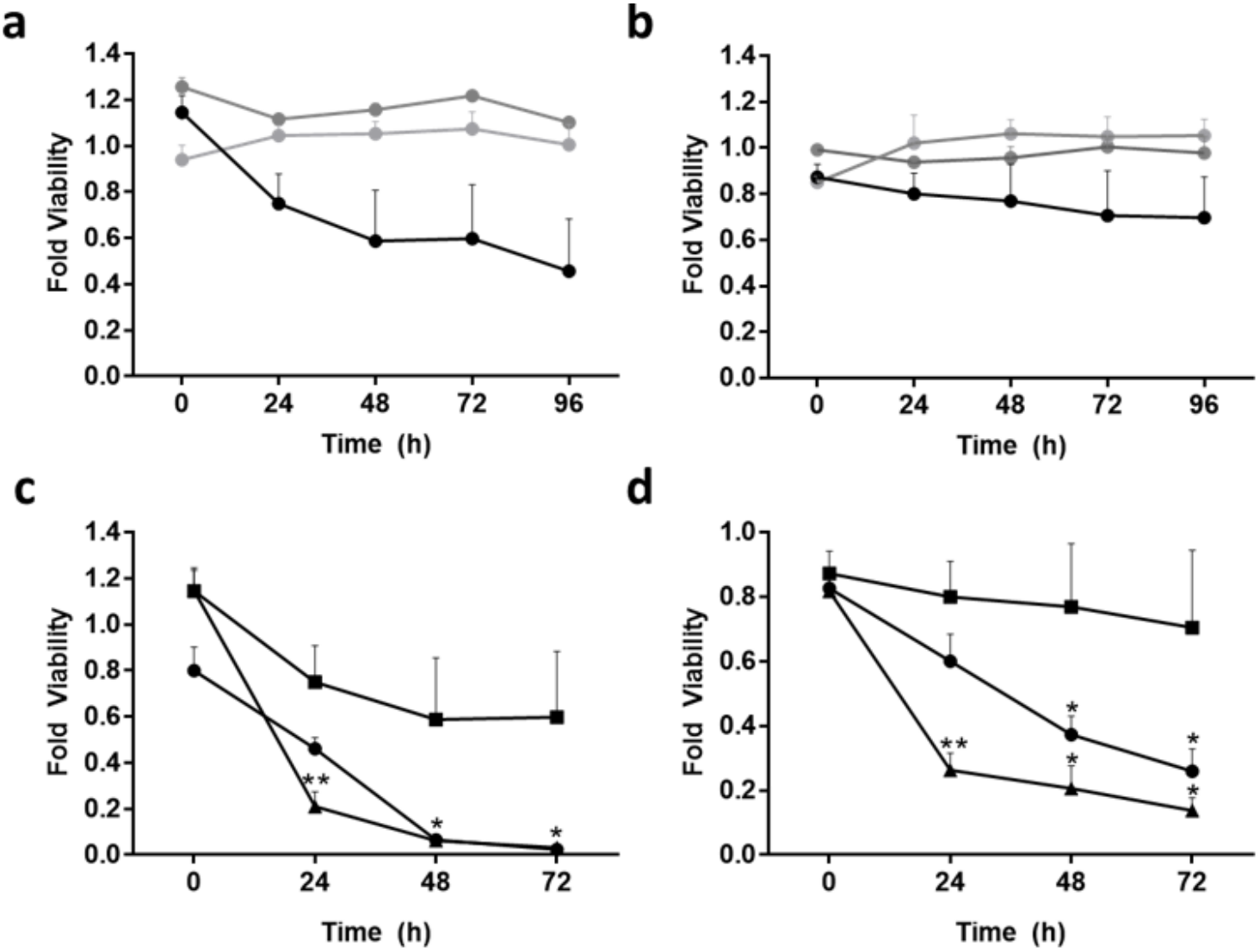

Figure 4

Nanoparticle systems cytotoxicity in in vitro Endometrial cancer models. RT-Glo viability curves for free drug (black), Empty NP (light grey) and Empty NP-HA (dark grey) at 2.5μM concentration for Ishikawa (a) and Hec50 (b) over a 96h period (N=4). All data are normalized to the untreated control cells. Encapsulated SAHA-NP drug systems cytotoxicity in vitro Endometrial cancer models. Monolayer cellular viability using Real Time Glo viability test (N=3) of SAHA Free Drug (square), SAHA-NP (triangle) an SAHA-NP-HA (circle) at the concentration of 2.5 μM for Ishikawa cell line (c) and Hec50 (d). All data was normalized to the untreated control cells.

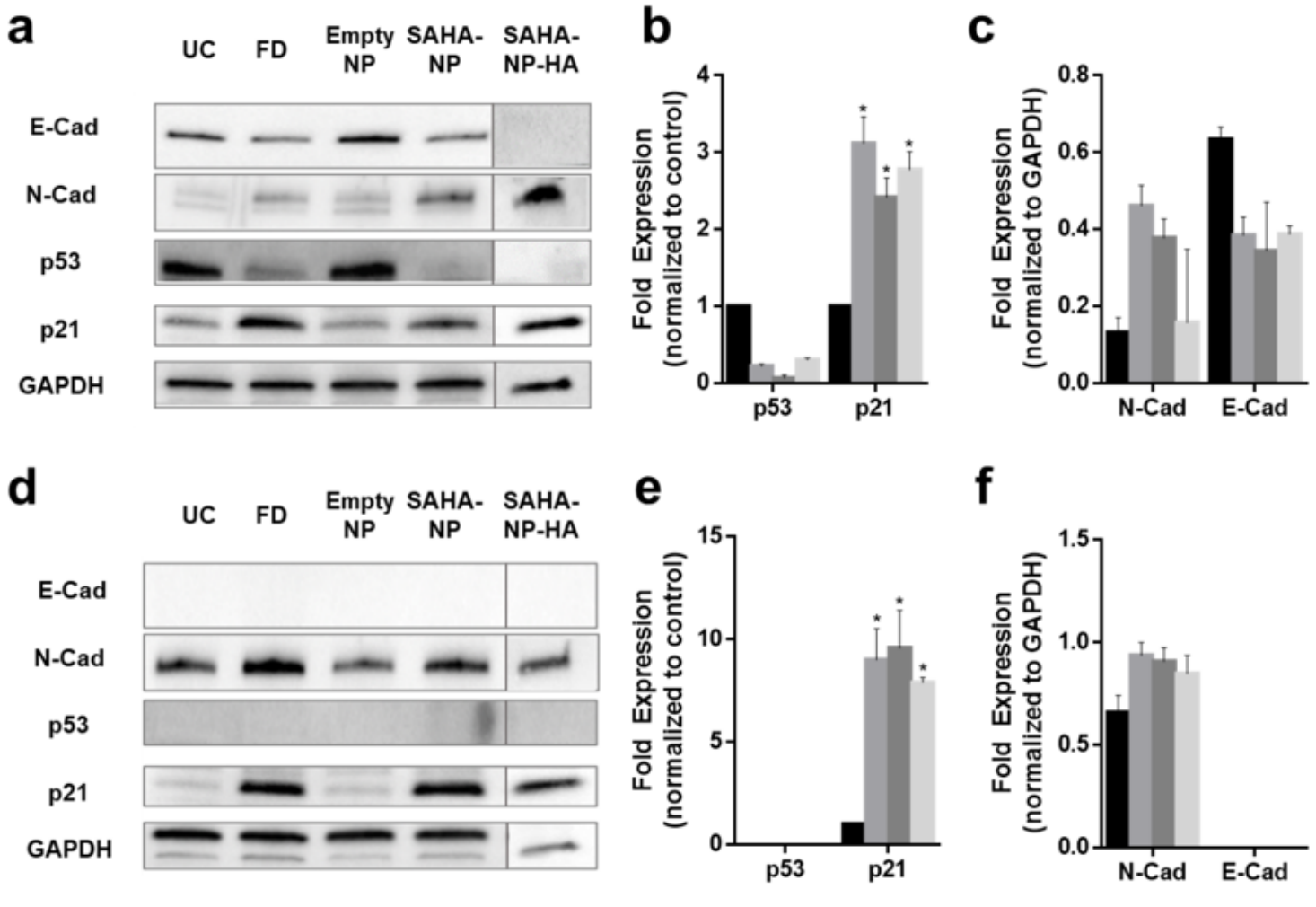

Figure 5

Effect of SAHA and encapsulated SAHA-NP drug systems on p21 and p53 expression and molecular phenotype from endometrial cancer cell line models. Representative example of Western Blots for Ishikawa (a) and Hec50 (d). Protein Densitometry graphs of media control (black) SAHA Free Drug (medium grey), SAHA-NP (dark grey) and SAHA-NP-HA (light grey) effects at the concentration of 2.5 μM for 72 hours for spheroids on cell cycle arrest markers p53 and p21 in Ishikawa (b) and Hec50 (e) and molecular phenotype markers E and N cadherin in Ishikawa (c) and Hec50 (f) , followed by protein dosimetry analysis. * P53 and p21 results are average and standard error, from a minimum of three independent biological repeats and are normalized to the untreated control cells and GAPDH protein density level. Cadherin values are average and standard error, from a minimum of three independent biological repeats normalized to GAPDH protein density level only.

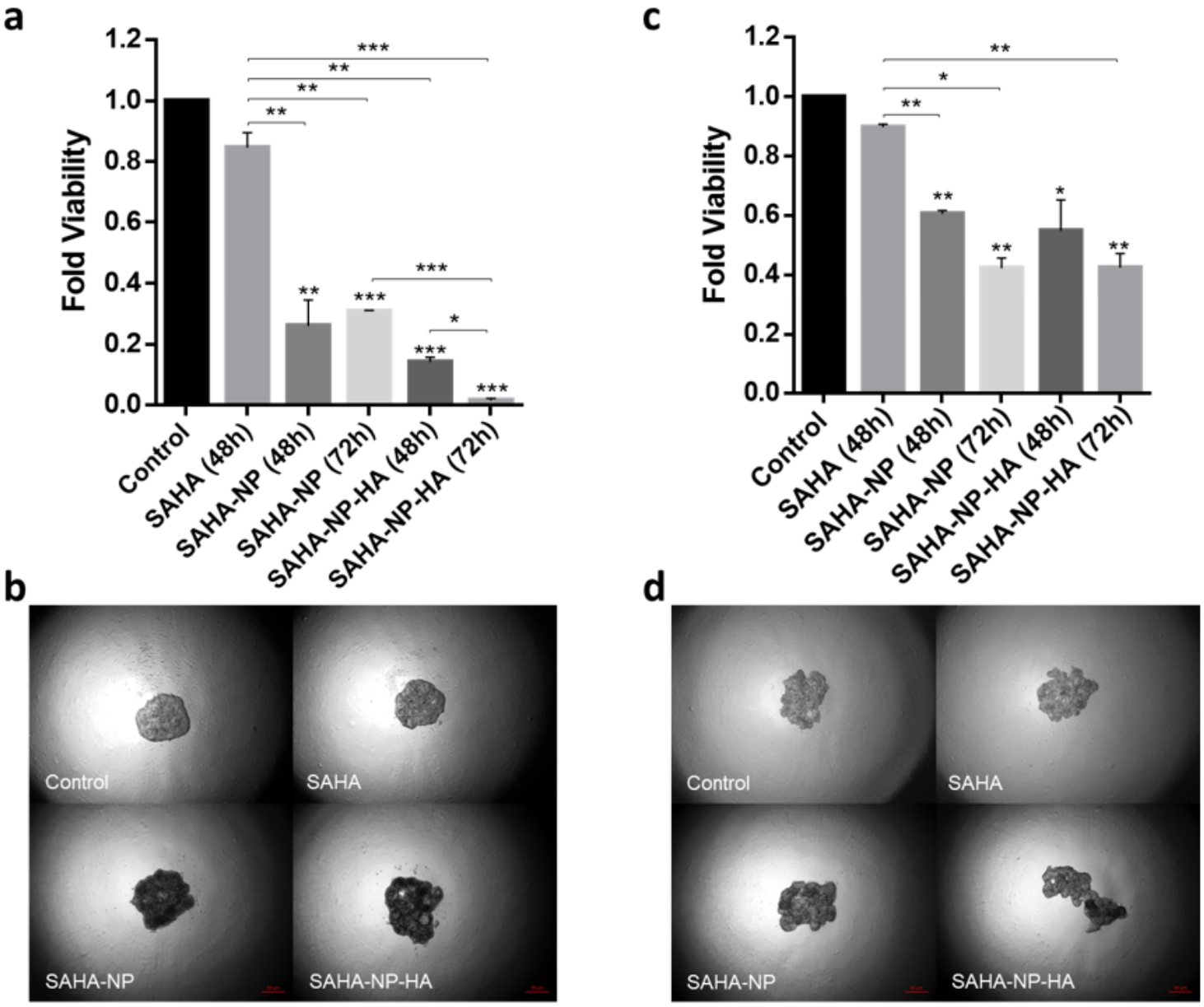

Figure 6

Encapsulated SAHA-NP drug systems cytotoxicity in vitro Endometrial cancer models. Spheroid cytotoxicity assessment using Celltiter Glo 3D (N=3) of SAHA Free Drug, SAHA-NP and SAHA-NP-HA at the concentration of 2.5 μM for 48h and 72h in Ishikawa (a) and Hec50 (c). All data is normalized to the untreated control cells. Images of Endometrial cancer model spheroids following treatment taken at 40X magnification. Images of Ishikawa (b) and Hec50 (d) control spheroids and spheroids treated with SAHA free, SAHA-NP and SAHA-NP-HA.

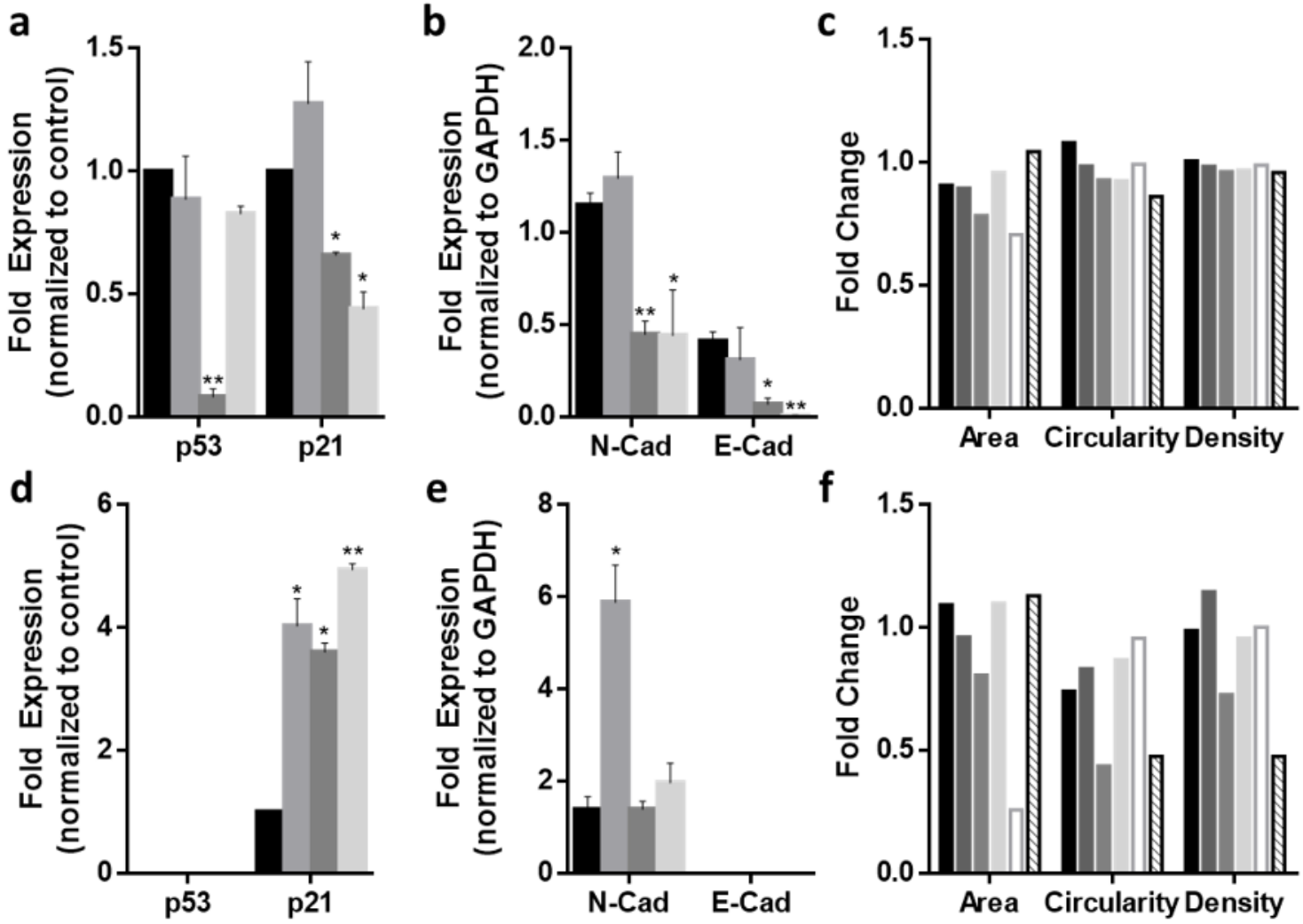

Figure 7

Effect of SAHA and encapsulated SAHA-NP drug systems on p21 and p53 expression and molecular phenotype from endometrial cancer cell line models. Protein Densitometry graphs of media control (black) SAHA Free Drug (medium grey), SAHA-NP (dark grey) and SAHA-NP-HA (light grey) effects at the concentration of 2.5 μM for 72 hours for spheroids on cell cycle arrest markers p53 and p21 in Ishikawa (a) and Hec50 (d) and molecular phenotype markers E and N cadherin in Ishikawa (b) and Hec50 (e) , followed by protein dosimetry analysis. * P53 and p21 results are average and standard error, from a minimum of three independent biological repeats and are normalized to the untreated control cells and GAPDH protein density level. Cadherin values are average and standard error, from a minimum of three independent biological repeats normalized to GAPDH protein density level only. Images of Endometrial cancer model spheroids following treatment taken at 40X magnification. ImageJ analysis of the spheroids was conducted to ascertain change in area, circularity and density in Ishikawa (c) and Hec50 (f) following treatments, free drug 48h (black), free drug 72h (dark grey), SAHA-NP 48h (medium grey), SAHA-NP 72h (light grey), SAHA-NP-HA 48h (white with grey outline) and SAHA-NP-HA 72h (striped). All data was normalized to untreated control spheroids.

Supplementary Files

This is a list of supplementary files associated with this preprint. Click to download.

- PluronicHAElectronicSupplementaryMaterials.docx
- PluronicHAElectronicSupplementaryMaterials.docx